The Effects of pK_a Tuning on the Thermodynamics and Kinetics of Folding: Design of a Solvent-Shielded Carboxylate Pair at the a-Position of a Coiled-Coil

Wai Leung Lau,[†] William F. DeGrado,[†*] and Heinrich Roder[†‡*]

[†]Department of Biochemistry and Molecular Biophysics, School of Medicine, University of Pennsylvania, Philadelphia, Pennsylvania; and [‡]Fox Chase Cancer Center, Philadelphia, Pennsylvania

ABSTRACT The tuning of the pK_a of ionizable residues plays a critical role in various protein functions, such as ligand-binding, catalysis, and allostery. Proteins harness the free energy of folding to position ionizable groups in highly specific environments that strongly affect their pK_a values. To investigate the interplay among protein folding kinetics, thermodynamics, and pK_a modulation, we introduced a pair of Asp residues at neighboring interior positions of a coiled-coil. A single Asp residue was replaced for an Asn side chain at the a-position of the coiled-coil from GCN4, which was also crosslinked at the C-terminus via a flexible disulfide bond. The thermodynamic and kinetic stability of the system was measured by circular dichroism and stopped-flow fluorescence as a function of pH and concentration of guanidine HCl. Both sets of data are consistent with a two-state equilibrium between fully folded and unfolded forms. Distinct pK_a values of 6.3 and 5.35 are assigned to the first and second protonation of the Asp pair; together they represent an energetic difference of 5 kcal/mol relative to the protonation of two Asp residues with unperturbed pK_a values. Analysis of the rate data as a function of pH and denaturant concentration allowed calculation of the kinetic constants for the conformational transitions of the peptide with the Asp residues in the doubly protonated, singly protonated, and unprotonated forms. The doubly and singly protonated forms fold rapidly, and a ϕ-value analysis shows that their contribution to folding occurs subsequent to the transition state ensemble for folding. By contrast, the doubly charged state shows a reduced rate of folding and a ϕ-value near 0.5 indicative of a repulsive interaction, and possibly also heterogeneity in the transition state ensemble.

INTRODUCTION

The folding and function of proteins reflects a delicate interplay between apolar (hydrophobic) and polar interactions. The burial of apolar residues provides a strong driving force for folding and substrate recognition (1,2), but the hydrophobic effect is generally less specific and geometrically directing than interactions between polar substituents (3). Burial of ionizable groups in an apolar (low-dielectric) environment gives rise to shifts in their pK_a values and concomitant free energy changes (4,5). Because of the energetic cost of burial (6), ionizable side chains are rarely found in the interior of proteins. However, there are a growing number of exceptions to this rule where internal ionizable groups and salt bridges play critical functional roles in processes such as redox reactions, ion transport, binding, and catalysis (e.g., (6–10)). Mechanistically, these activities often make use of shifts in pK_a values, which can be large for an ionizable group in an apolar environment. Here we examine the effect of an engineered Asp/Asp pair on the pH-dependence of the kinetics and thermodynamics of folding of a simple coiled-coil peptide.

Buried polar interactions are important for conformational specificity (i.e., the tendency of a protein to adopt a single set of conformations in preference to a multitude of alternative, misfolded structures). The dehydration of polar groups is unfavorable and often compensated for by forming hydrogen-bonded interactions that restrict the geometric relationships of the interacting groups (e.g., (11–14)). For example, Asn^{16} in the a-position of a coiled-coil domain, GCN4-p1, confers specificity for dimer formation (15). Substitution of the Asn^{16} by a nonpolar amino acid leads to peptides that, although thermodynamically more stable, tend to form higher order oligomers (16). In other GCN4 variants, replacement of hydrophobic amino acids at the helical interface by glutamine was found to promote trimer formation (17).

Additional features come into play when the buried group is ionizable, because the dehydration of a charged group is more unfavorable, leading to an even stronger tendency to interact with other side chains and/or ligands. For example, intramolecular salt bridges help compensate for the burial of charged groups, thereby contributing to the discrimination of the native fold relative to alternative conformations (18). In addition, partially buried carboxylates are often involved in receptor-ligand interactions and serve important roles as general acids/bases in the active site of enzymes. In particular, interacting Asp and Glu residues are frequently encountered in enzymes and transporters, in which protons or metal ions are bound or shuttled during the course of translocation or catalysis (7,9). Classical examples include the Asp/Glu pairs found in the acid protease pepsin (19), HIV protease (20), and bacteriorhodopsin (10). These are examples of the well-known

Submitted June 2, 2010, and accepted for publication July 29, 2010.

*Correspondence: wdegrado@mail.med.upenn.edu or h_roder@fccc.edu

Editor: George I. Makhatadze.

0006-3495/10/10/2299/10 $2.00

doi: 10.1016/j.bpj.2010.07.059

stability/function tradeoff, which postulates that proteins sacrifice global stability to allow the formation of binding and catalytic sites, and to modulate the chemical properties within these sites (21).

The pK_a of interacting carboxylates are strongly modulated due to their mutual proximity, dehydration, and hydrogen-bonding interactions between protonated and nonprotonated forms of a carboxylate (e.g., (22–25)). These factors can strongly increase the affinity of a proton for the first of two closely interacting carboxylates, leading to large upward shifts in pK_a relative to a carboxylate in aqueous solution. Monoprotonation relieves the electrostatic repulsion between the two carboxylates, and decreases the unfavorable dehydration energy associated with burial of the group. The second pK_a is also likely to be increased, if the two groups are largely shielded from water.

In this work, we examine the effect of changing a pair of interacting Asn side chains to Asp residues in the dimeric coiled-coil from GCN4. This is a particularly well-studied and simple protein; its protonation equilibrium is well established (26,27), and the effects of mutations on its structure (15,16,28–30) and folding kinetics (31–37) have been investigated in detail. In the crystal structure of the native coiled-coil dimer of GCN4 (15), one Asn residue from each chain interacts to form an interchain hydrogen bond near the center of the protein (Fig. 1, *A–C*). In the predominant conformation, the side chains interact asymmetrically, with each Asn adopting a different set of $\chi 1$ and $\chi 2$ angles to allow hydrogen-bonding between the carboxamide amide NH_2 of one Asn and the carbonyl of the other (15). Each Asn side chain also engages in an additional hydrogen bond; one accepts a hydrogen bond from a solvent water molecule while the other donates a hydrogen bond to a main-chain carbonyl oxygen of the neighboring helix (Fig. 1 *B*). A second symmetrical set of rotamers is also possible, based on a high-resolution crystallographic analysis of a closely related peptide (38). Although this rotameric state is probably less populated in the native structure, it might be important when Asn is mutated to Asp. This conformation positions the side chains further apart from one another, creating a cavity about the size of one or two water molecules (Fig. 1 *C*). Thus, depending on the ionization state of the Asp side chain, it might be accommodated in one of two conformations, both of which are partially, but not fully shielded from the solvent (side chains not shown in Fig. 1 partially occlude the exposure of the Asn to solvent).

To understand the influence of partially buried polar amino acids on specificity of coiled-coil assembly, Knappenberger et al. (36) investigated the thermodynamics and folding kinetics of GCN4-p1 and two of its variants in which the Asn^{16} was replaced by either an alanine or a valine. Their observation that these peptides exhibit very similar folding rates, but widely different unfolding rates indicates that the mutations do not significantly perturb the free energy of the transition state relative to the unfolded state, and that the Asn side chain is not involved in the rate-determining step of the folding reaction. Here we explore the folding mechanism of GCN4-D, a single-chain two-helix coiled-coil formed by cross-linking two GCN4 Asp-p1 peptides via a pair of Cys introduced near the C-terminus (39). An important design element of GCN4-D is that the Asn residues at the helix-helix interface (Fig. 1 *A*) are replaced by Asp (Asp^{18} in our sequence). This feature allows us to vary continuously the interaction energy between the two Asp residues in GCN4-D by changing the pH. Quantitative kinetic analysis based on a six-state model (Fig. 1 *D*) allowed us to determine the thermodynamic and kinetic properties of three distinct forms of the protein with different combinations of charges on the central pair of Asp side chains. In analogy to mutational studies, a ϕ-value (40) or ψ-value (35) analysis of the kinetic data provides information on the interactions involved in stabilizing the transition state for folding.

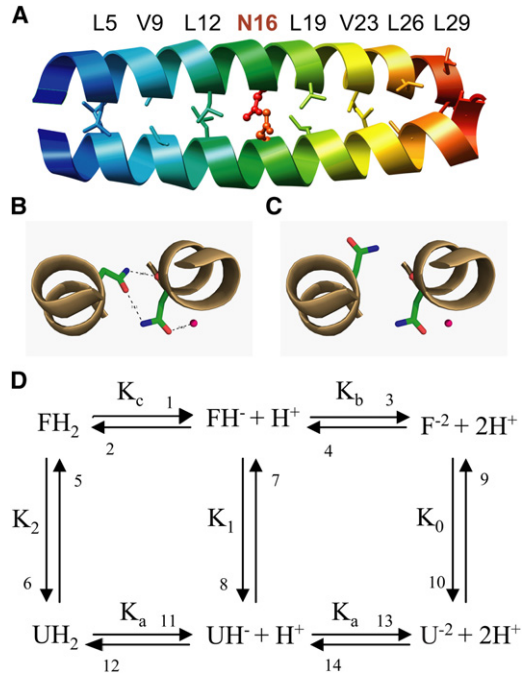

FIGURE 1 (*A*) Ribbon diagram of the coiled-coil dimer of GCN4-p1 (30). The buried Asp^{16} is shown in ball-and-stick representation. (*B*) Expanded diagram based on the crystal structure of Deng et al. (30), showing hydrogen-bonded interactions of Asp^{16}. The sphere indicates a water molecule. (*C*) Alternative conformation of Asp^{16} as seen in the crystal structure of a GCN4/cortexillin hybrid coiled-coil peptide (38). (*D*) A six-state model that describes the coupled folding and ionization equilibria of cross-linked GCN4-D. F^{-2} represents the folded coiled-coil conformations in which the two buried Asp residues are deprotonated, and FH^- and FH_2 are the single- and double-protonated forms. U^{-2}, UH^-, and UH_2 are the corresponding unfolded states. K_0, K_1, and K_2 are equilibrium constants for unfolding of each species. K_a is the ionization constant for the buried aspartate (Asp^{18}) in the unfolded state; K_b and K_c are ionization constants for each Asp^{18} in the SS-linked GCN4-D dimer. Numbers next to the arrow refer to elementary rate constants for each transition.

MATERIALS AND METHODS

Solvents and other reagents for peptide synthesis were obtained from Sigma-Aldrich (St. Louis, MO). Nine-fluorenylmethoxycarbonyl (Fmoc) amino acids were purchased from Novabiochem (Darmstadt, Germany). Two-[*n*-Cyclohexylamino]-ethanesulfonic acid, 2-(*n*-morpholino)ethanesulfonic acid (MES), 3-[*n*-Morpholino]propanesulfonic acid, sodium acetate, and glycine were purchased from Sigma-Aldrich. Guanidine hydrochloride (GuHCl) was purchased from Fisher Scientific (Fairlawn, NJ) and Pierce (Rockford, IL).

Peptide synthesis and purification

The GCN4-D peptide employed in this study has the sequence

GGRMKQLEDK^{10}VEELLSKDWH^{20}LENEVARLKK^{30}

LVGERGGCG.

This peptide was synthesized using a standard solid-phase Fmoc method on a model No. 433A peptide synthesizer (PE Applied Biosystems, Foster City, CA). After synthesis, the N-terminal Fmoc group was deprotected by 20% (v/v) piperidine to generate a free amino terminus which is then coupled with acetic anhydride in 10-fold excess of pyridine and dimethylformamide for 30 min. The peptide was cleaved from the resin using trifluoroacetic acid with thioanisole, ethanedithiol, and anisole in the 90:5:3:2 (v/v). Before purification, the Cys was reduced to thiol using dithiothreitol. GCN4-D monomer was purified to homogeneity by reverse-phase high pressure liquid chromatography (HPLC) using a C4 column (22 × 250 mm, 10-μm particle size; Grace Vydac, Hesperia, CA) running a binary, linear gradient of 35–42% B in 30 min. Buffers A and B are water and acetonitrile/water in the ratio 9:1 (v/v), respectively, in the presence of 0.1% trifluoroacetic acid by volume. To generate disulphide cross-linked dimer, the GCN4-D monomer (1 mg/mL) was dissolved in 100 mM 2-[*n*-Cyclohexylamino]-ethanesulfonic acid at pH 8.0 and stirred under open air. Oxidation of the cysteine resulted in the formation of homodimer. The reaction product was fractionated using the reverse-phase HPLC. The purity of the dimer was determined by analytical HPLC. The identity of the homodimer was confirmed by matrix-assisted laser desorption/ionization-time-of-flight mass spectrometry using a Voyager DE-RP Biospectrometry Workstation (PerSeptive Biosystems, Framingham, MA).

Equilibrium denaturation experiment

The dependence of stability of GCN4-D on pH was studied by circular dichroism (CD) spectroscopy. At a given pH, GCN4-D peptide in 150 mM NaCl and 10 mM buffer (sodium acetate for pH 4.8–5.4, MES for pH 5.7–6.2) was titrated with peptide dissolved in the same buffer containing high concentrations of GuHCl. For each final denaturant concentration, the ellipticity at 222 nm was averaged for at least 60 s. Experiments were conducted at 10°C, the same temperature as in the kinetics experiment. The concentration of the GuHCl in buffer was determined by refractive index measurement using a refractometer. Peptide concentrations were determined from UV absorption measurement in 6 M GuHCl, ε_{280} = 5600 M^{-1} cm^{-1}. Procedures for analysis of the equilibrium denaturation experiment are described in the Supporting Material.

Stopped-flow kinetics

Folding/unfolding buffers were prepared by mixing stock solutions of sodium chloride, deionized water, GuHCl, and either sodium acetate or MES. The buffers were titrated to the desired pH (4.8, 5.2, 5.7, or 6.2) using either hydrochloric acid or sodium hydroxide. After mixing, buffers and peptide solutions were degassed under vacuum and filtered. Concentrations of GuHCl in the buffers were determined by refractive index measurements.

Folding and unfolding kinetics were measured at 10°C using a model No. SF-4 stopped-flow spectrofluorimeter (BioLogic Science Instruments, Claix, France). The unfolding reaction was initiated by rapid dilution of a peptide solution (90 μL of ~90 μM solution) into five volumes of unfolding buffers. Similarly, the refolding reaction was triggered by mixing peptide solution containing high concentration of GuHCl with refolding buffer. For each reaction, at least five kinetic traces recorded on a log timescale were averaged to give the final kinetic trace. Samples were collected after each mixing reaction for refractive index and pH measurements. Excitation of the tryptophan was set at 284 nm and emission was measured using a 324-nm cut-on filter. In a second series of experiment, the unfolding kinetics at constant final GuHCl concentration (3.5 M, 3.75 M, and 4 M) as a function of pH was studied. Procedures for analysis of the refolding and unfolding kinetics are described in the Supporting Material. To acquire data that represent the limiting case of folding of the peptide with both of the buried aspartic acids protonated, experiments were done at pH 2.7 using glycine buffer.

RESULTS

Modifications to GCN4-p1

The GCN4-p1 variant employed in this study, GCN4-D, has the sequence (subscripts indicate heptad repeat positions).

GGR M_aKQL$_d$EDK V_aEEL$_d$LSK $\mathbf{D}_a$WHL$_d$ENE V_aARL$_d$KKL V_aGER$_d$ GGCG.

Residues 3–35 are derived from GCN4 Asp-p1 (39). Following Sosnick et al. (32), the Trp^{19} of this peptide replaces Tyr^{19} in GCN4-p1, providing a convenient fluorescent tag for monitoring its folding. Crosslinking of the two helices by disulfide bond formation at the cysteine residue makes the folding process unimolecular. The Gly residues serve as a flexible linker between the GCN4-p1 and the cysteine. Disulfide formation further insures a parallel coiled-coil arrangement of the two helices. This results in a pair of partially buried Asp side chains at position 18 near the center of the coiled-coil dimer (Fig. 1 *A*).

Stability of GCN4-D versus pH

To determine the effect of pH on the structural stability of GCN4-D, we used CD to monitor the GuHCl-induced unfolding transitions versus pH (Fig. 2). The results at 10°C (Fig. 2 *A*) show that the stability of GCN4-D decreases strongly with increasing pH over the range from 4.8 to 6.2. In contrast, we previously found that the stability of GCN4-p1 was relatively insensitive to pH from 4.5 to 6.0 (39), indicating that the buried Asp at position 18 dominates the effect of pH on stability over this range. The denaturation curves are sigmoidal in shape and show a decrease in the midpoint concentration, C_m, with increasing pH. Qualitatively similar results were obtained in CD-detected

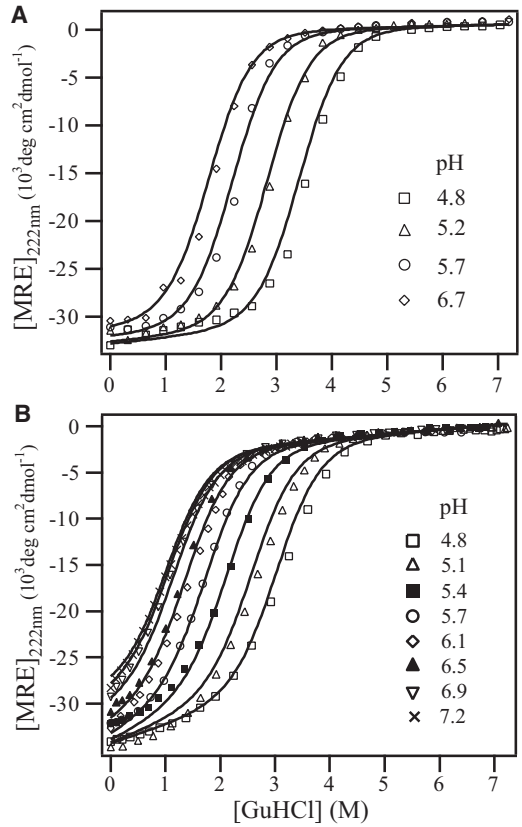

FIGURE 2 Unfolding equilibrium of GCN4-D as a function of denaturant concentration and pH monitored by far-UV CD. The mean residue ellipticity at 222 nm, $[\theta]_{222}$, measured at 10°C (*A*) and 25°C (*B*) is plotted versus GuHCl concentration at different pH values. (*Solid lines*) Global fit to a six-state model (Fig. 1 *D*), using the kinetically derived parameters as constraints (Table 1).

equilibrium measurements at 25°C, covering a wider range of pH values (Fig. 2 *B*).

The denaturant-induced unfolding equilibrium of GCN4-D was globally analyzed using a six-state model (Fig. 1 *D*) consisting of folded (F) and unfolded (U) conformations for each of three ionization states in which the pair of buried Asp side chains is fully deprotonated (F^{-2}/U^{-2}), singly-protonated (FH^{-}/UH^{-}), or fully protonated (FH_2/UH_2), respectively. After considering thermodynamic reversibility, this scheme required a total of five adjustable thermodynamic equilibrium constants. The pK_a for protonation of Asp^{18} in the unfolded state, pK_a, was assigned a value of 4.1 (typical unperturbed pK_a of Asp). The remaining three equilibrium constants and baseline were globally fit as described in Materials and Methods, using both the equilibrium and kinetic data.

The calculated free energy of unfolding decreases in the order

$$FH_2 \rightarrow UH_2 > FH^{-} \rightarrow UH^{-} > F^{-2} \rightarrow U^{-2},$$

consistent with the expectation that the folded coiled-coil structure is stabilized by interactions between protonated Asp side chains at the helix-helix interface and strongly destabilized by interactions between negatively charged Asp side chains (Table 1). The pK_a for dissociation of the doubly protonated Asp pair is 5.65 ($\Delta pK_a = 1.45$); the corresponding value for the dissociation of the singly protonated Asp pair is 6.3 ($\Delta pK_a = 2.2$). These values represent a large energetic change corresponding to $\Delta\Delta G = 2.0$ and 2.8 kcal/mol, respectively, or a total stability difference of ~5 kcal/mol.

The kinetics of GCN4-D folding and its dependence on pH

Fig. 3 *A* shows a semilogarithmic plot of the observed folding and unfolding rates versus concentration of denaturant (chevron plot) at four pH values from 4.8 to 6.2 (additional data at pH 2.8 are included in Fig. S1 in the Supporting Material). The results obtained reveal the following features.

First, the observed refolding and unfolding rates intersect near the midpoint of the equilibrium unfolding curves (Fig. 2), indicating that the reaction is reversible.

Second, the curves are linear above and below the minimum, indicating that no spectroscopically distinct intermediates accumulate during the folding/unfolding process (within the range of guanidine concentrations employed). This indicates that, in terms of structure (but not charge state), the system can be described by a two-state model.

Third, the minimum of the V-shaped curve shifts to lower GuHCl concentration as the pH is increased. Because the minimum corresponds to the midpoint of the unfolding equilibrium in a two-state model, this observation indicates that the stability of GCN4-D decreases with increasing pH, consistent with our equilibrium denaturation experiments.

TABLE 1 Elementary rate constants, *m* values, and equilibrium parameters describing the folding/unfolding kinetics of GCN4-D at 10°C

Transition ($i \rightarrow j$)	$UH_2 \rightarrow FH_2$	$FH_2 \rightarrow UH_2$	$UH \rightarrow FH^{-}$	$FH \rightarrow UH^{-}$	$U^{-2} \rightarrow F^{-2}$	$F^{-2} \rightarrow U^{-2}$
k_{ij} (s^{-1})	60,000	0.19	67,000	7.5	5500	98
m_{ij} (kcal mol^{-2} L)	−0.87	0.6	−0.93	0.54	−1.12	0.35
α	0.59		0.63		0.76	
ΔG (kcal mol^{-1})	7.1		5.1		2.3	

The pK_a values of the buried Asp^{18} in the folded dimer are 5.65 ($FH^{-} \leftrightarrow FH_2$) and 6.3 ($F^{-2} \leftrightarrow FH$), respectively. A pK_a of 4.1 was assumed for protonation of Asp^{18} in the unfolded state. For each charge state, $\alpha = -m_{ij}/(m_{ji}-m_{ij})$, where m_{ij} and m_{ji} are the kinetic *m* values for folding and unfolding, respectively.

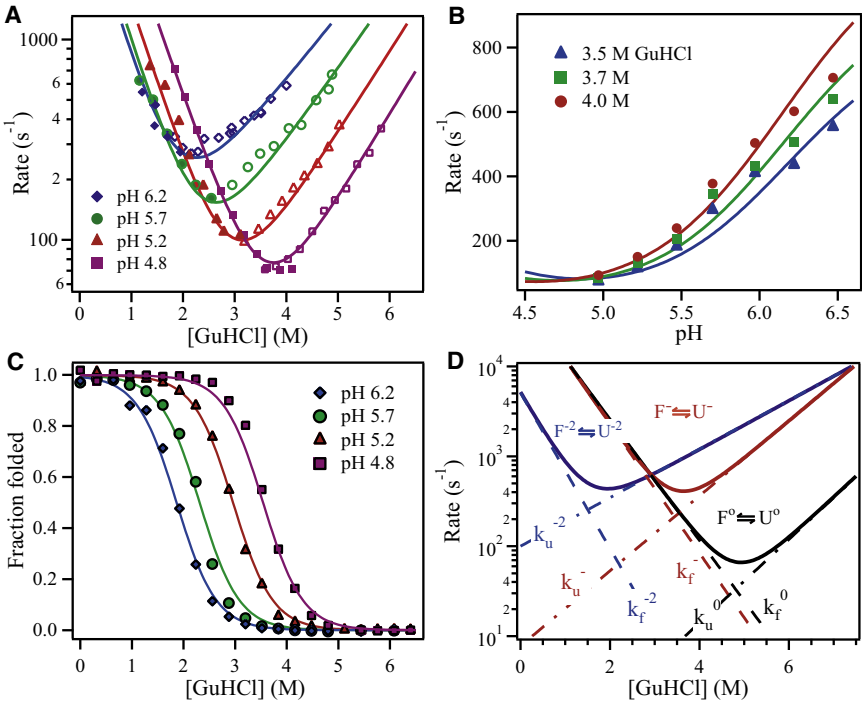

FIGURE 3 (*A*) Semilogarithmic plots of the observed folding/unfolding rate constant of GCN4-D at 10°C versus GuHCl concentration (*chevron plot*). Rate constants for folding (*solid symbols*) and unfolding (*open symbols*) were measured by stopped-flow fluorescence at pH 4.8 (*squares*), 5.2 (*triangles*), 5.7 (*circles*), and 6.2 (*diamonds*). (*Solid lines*) Modeling of the kinetic data using numerical analysis according to a six-state kinetic scheme. In this simulation, the rate of diffusion of hydrogen ions is arbitrarily set to 10^{12} s^{-1}. (*B*) Plot of observed unfolding rates versus pH, obtained at a final GuHCl concentration of 3.50 (△), 3.75 (□), and 4.00 M (○). (*Solid lines*) Fit of the observed unfolding rates to the six-state kinetic scheme, using the kinetic parameters obtained from simulating the chevron plot in panel *A*. (*C*) Plot of fraction of folded GCN4-D versus GuHCl concentration, measured by circular dichroism at pH 4.8 (■), pH 5.2 (▲), pH 5.7 (●), and pH 6.2 (◆). (*Solid lines*) Theoretical curves computed on the basis of kinetic parameters obtained from simulating the kinetic data in Fig. 2 *a*. (*D*) Plot of elementary folding and unfolding constants as a function of GuHCl concentration for the neutral, −1 charged, and −2 charged species (*dashed lines*). (*Solid lines*) Theoretical chevron plot for the neutral, −1 charged, and −2 charged species, assuming 100% population, computed on the basis of kinetic parameters obtained from simulating kinetic data in panel *A*. (*Dashed lines*) Elementary rate constants as a function of GuHCl concentration.

Fourth, an increase in pH causes a large increase in unfolding rates and a more moderate decrease in refolding rates. Thus, the thermodynamic destabilization of the folded protein with increasing pH is primarily a consequence of increasing the rate of unfolding rather than slowing the rate of folding. This conclusion is further supported by comparing the folding/unfolding kinetics of GCN4-D with published results on GCN4-p2′, an N-terminally crosslinked construct with the wild-type Asn at position 18 studied by Moran et al. (41) under conditions similar to ours (pH 5.5, 10°C). The folding arm of the chevron plot of GCN4-p2′ closely matches that of GCN4-D, but unfolding rates are ~50-fold slower, accounting for the stabilization due to the more favorable Asn[18].

By using numerical analysis (see the Supporting Material), we explored the kinetic behavior predicted by our six-state model (Fig. 1 *D*), assuming that the dependence of each elementary folding and unfolding rate constant, k_j, on denaturant concentration, c, can be described as

$$k_j = k_j^o \exp(m_j \cdot c/RT),$$

where m_j is the kinetic m value, R is the gas constant, and T is the absolute temperature (e.g., (42)). The rate constant for protonation and deprotonation of acidic groups (i.e., each of the two Asp side chains) were assumed to be independent of the denaturant concentration. To determine whether the rate of protonation or deprotonation was rapid relative to the conformational steps, the second-order rate constant for protonation was systematically varied; satisfactory fits to the experimental data were obtained as long as the rate was >~10^9 M^{-1} s^{-1} (Fig. S3 *D*). Strong deviations were observed when the rate constant was decreased below this value, placing a lower limit of 10^9 M^{-1} s^{-1} on this parameter. The value of the corresponding deprotonation rates (k_1, k_3, k_{11}, k_{13} in Fig. 1 *D*) were also found to be >10^3 s^{-1}, faster than the observed conformational processes measured. Thus, the rate of interconversion between different protonation states in the folded ensemble as well as the unfolded ensemble is fast compared to the rate of interconversion between folded and unfolded states. This observation is consistent with the finding that rotamer interconversion of Asn[16] was rapid in the WT peptide (43). This also simplifies the fitting procedure, as each protonation/deprotonation step can be treated as a rapid equilibrium with a single dissociation constant rather than requiring specification of both a forward and reverse rate constant.

The parameters describing each of the microscopic rate constants relating the six states, k^o_j and m_j, were varied manually, and the predicted rates were compared with the data in an effort to simultaneously fit the observed refolding/unfolding rates at all pH values and denaturant concentrations. The optimized set of kinetic parameters obtained

(Table 1) resulted in an excellent simultaneous fit of the chevron curves at each pH value (Fig. 3 *A*, *solid lines*), indicating that the six-state kinetic scheme is fully consistent with our kinetic data. Moreover, the same set of kinetic parameters also approximates the observed unfolding rates as a function of pH, measured at constant final GuHCl concentration of 3.5, 3.75, and 4.0 M (Fig. 3 *B*; a small deviation near pH 6.2 might reflect a change in protonation of His^{37}, which was also observed in the WT protein). In addition, we computed theoretical equilibrium transition curves using the kinetic parameters in Table 1 and compared them with the equilibrium denaturation curves monitored by CD (Fig. 2 and Fig. 3 *C*). The agreement between the theoretical and experimental curves is excellent, indicating that our six-state model (Fig. 1 *D*) is sufficient to describe the folding of GCN4-D under our experimental conditions. Thus, the final set of kinetic parameters (Table 1) is well constrained by the global fit of the observable folding/unfolding rate constants and equilibrium data versus denaturant concentration and pH (Fig. 3), as well as the mass-balance relations.

To determine the uniqueness of this mechanism, we have explored two alternative models. A simplified four-state model (Fig. S2 *A*) would be adequate if only two of the three folded species and their unfolded counterparts predominate under the experimental conditions used. Another alternative to the six-state scheme is a four-state model in which the two Asp^{18} residues take up or release their protons in a cooperative manner (Fig. S2 *B*). However, both of these alternative models fail to satisfy simultaneously the equilibrium and kinetic data. The first scheme (Fig. S2 *A*) fits the pH-dependent equilibrium unfolding transitions (data not shown), but fails to reproduce the gradual decrease in the slope of the unfolding arm in the chevron plot as the pH is increased from 4.8 to 6.2 (Fig. S3, *A* and *B*). The cooperative model (Fig. S2 *B*) provides an adequate description of the equilibrium transitions (data not show), but again leads to a poor fit of the kinetic data (Fig. S3 *C*). In contrast, we were able to quantitatively model the equilibrium denaturation curves (Fig. 2, *solid lines*) as well as all available kinetic data (Fig. 3), indicating that the full six-state scheme (Fig. 1 *D*) is the minimal model consistent with the thermodynamics and kinetics of GCN4-D folding.

DISCUSSION

The ability to finely tune the pK_a of ionizable groups is an important feature in the design of functional proteins. Here, we examine the effect of environment on the pK_a of a pair of Asp residues at an interior-facing a-position of a coiled-coil. In contrast to other polar and charged residues, Asp is rarely found at the buried a- or d-positions of coiled-coils (44). In a search of the database of coiled-coil structures maintained by Testa et al. (45), we found 36 occurrences of Asn, but only a single case of Asp at the a-position of parallel two-strand coiled-coils, a noncanonical coiled-coil domain studied by Lee et al. (46); i.e., PDB ID 3e1r. When placed at the a-position by mutagenesis, Asp is highly destabilizing (44,47). However, with its covalently linked pair of strands, GCN4-D is stable enough to tolerate Asp at this core position. Although the corresponding Asn residues in the WT protein are frequently considered to be fully buried, they have a small amount of solvent-exposure and can form hydrogen bonds to solvent in crystal structures of the protein (Fig. 1 *B*). Indeed, in this study, we find the rate of protonation/deprotonation of Asp^{18} is relatively rapid, which has simplified the kinetic analysis.

Many previous studies examined charged groups in more solvent-accessible e-, g-, and c-positions of coiled-coils (28,37,48–56). A high degree of specificity can be achieved by manipulating the charges at a large number of positions; however, on a per-residue basis, the thermodynamic effect of each side chain is much smaller than that observed here. By mutating a less solvent-exposed residue, much larger perturbations in the pK_a of acidic groups are observed in this study, amounting to ~5 kcal/mol for protonation of the two side chains in the native versus unfolded states. The strongly perturbed pK_a values presumably reflect several effects that are difficult to separate, but most likely include contributions from partial dehydration of the carboxylate, relief of unfavorable carboxylate/carboxylate interactions (for the first protonation), and possibly a hydrogen bond between the two protonated carboxyl groups, as in the WT protein with Asn at these two positions (Fig. 1 *B*).

The relationship $\alpha^{\ddagger} = -m_f/(m_u - m_f)$, where m_f and m_u represent the kinetic m values for folding and unfolding of each charge state, allows us to determine the position of the transition state in relation to the folded and unfolded states in Fig. 1 *D*. Because m values reflect the change in solvent-accessible surface area associated with a conformational transition, the $\alpha^{\ddagger}$-value reflects the average degree of solvent exposure of the transition state for folding of each species relative to the unfolded ($\alpha^{\ddagger} = 0$) and native states ($\alpha^{\ddagger} = 1$). The $\alpha^{\ddagger}$-values obtained for FH_2, FH^-, and F^{-2} are 0.59, 0.63, and 0.76, respectively, indicating that the solvent accessibility of the transition state ensemble on the reaction coordinate decreases in the order $FH_2 > FH^- > F^{-2}$. The value of 0.59 for the FH_2 state is in good agreement with that measured for variants of GCN4-P1, with Asn at the corresponding positions of Asp^{18} and $Asp^{18\prime}$ (57). Although it is possible that the change in $\alpha^{\ddagger}$ reflects deviations from two-state behavior, a variety of other measures, including the solvent deuterium isotope effects, also show that a similar fraction of structure is formed for GCN4-P1 in the transition state ensemble (58), irrespective of the helical potential of the sequence. It is therefore interesting that the transition state of F^{-2} resembles the native state more closely than that of FH^- and FH_2. On the other hand, ΔC_p values measured by thermal unfolding suggest a lower degree of solvent exclusion in the transition-state ensemble of GCN4

(59), which might reflect the difference between accessibility to guanidine (α-factor) compared to the smaller water molecules.

Our kinetic analysis has made it possible to isolate the folding rates for the different protonation states, which can be treated like a set of point mutations and subjected to conventional ϕ-value analysis. Each isolated charge state exhibits a simple V-shaped rate profile (Fig. 3 *D*), and can thus be characterized by a two-state free energy profile with a single barrier (Fig. 4 *C*). To determine the perturbations in transition-state free energy due to electrostatic interactions or potential hydrogen bonds involving Asp^{18}, we determined Φ-values analogous to those used to characterize mutational effects (40,60). Mutant Φ-values for the transition state in folding of a two-state protein are defined as

$$\varphi = \frac{\left(\Delta G^{\ddagger}_{\mathrm{wt}} - \Delta G^{\ddagger}_{\mathrm{mut}}\right)}{\left(\Delta G^{\mathrm{eq}}_{\mathrm{wt}} - \Delta G^{\mathrm{eq}}_{\mathrm{mut}}\right)} = \frac{-RT\cdot\ln\left(k_f^{\mathrm{wt}}/k_f^{\mathrm{mut}}\right)}{\left(\Delta\Delta G^{\mathrm{eq}}_{\mathrm{mut}}\right)}, \qquad (1)$$

where $\Delta G^{\ddagger}_{\mathrm{wt}}$ and $\Delta G^{\ddagger}_{\mathrm{mut}}$ are the free energies of the folding transition state relative to U, $\Delta G^{\mathrm{eq}}_{\mathrm{wt}}$ and $\Delta G^{\mathrm{eq}}_{\mathrm{mut}}$ are unfolding free energies, and k_f^{wt} and k_f^{mut} are folding rate constants for the wild-type and mutant, respectively. In our case, we treat the protonation of an Asp like a mutation, comparing the kinetics of FH^- (mutant) to FH_2 (wild-type), and that of F^{-2} (mutant) to FH^- (wild-type). Using parameters from kinetic modeling (Table 1), the Φ-value for conversion of FH_2 to FH^- is -0.03 (essentially 0, considering experimental and extrapolation errors (61)). This suggests that, proceeding from the unfolded to the folded state, the interactions between Asp^{18}-$Asp^{18\prime}$ are formed only after crossing the folding barrier. In contrast, for the second deprotonation step (FH^- to F^{-2}) we obtain a Φ-value of 0.50 (relative to the wild-type FH^-). Apparent Φ-values are somewhat dependent on GuHCl concentrations, and the values presented are those in the absence of denaturant.

The transition state ensemble for the folding of coiled-coils is heterogeneous, and dependent on the local stability of specific sites along the chain as well as the presence of cross-links in the sequence (35,57,58). In this work, the peptides are cross-linked at the C-terminus, which increases the helical content near the C-terminal region of the helix in the transition state ensemble for unfolding (35). Thus, our finding of a low or fractional ϕ-value for the differing protonation states of Asp^{18} is consistent with the previously reported small degree of structure in this region of chain in the TS ensemble, when the C-terminal region is crosslinked (35). This finding is also consistent with the previous findings of relatively high local stability near the C-terminus of GCN4-p1 (33), and the very fast folding of N-terminally truncated forms of this peptide (62,63).

Finally, pH variation makes it is possible to continuously vary the stability of the protein over a wide range by modulating the energetics associated with tertiary interactions between a pair of small residues. In this regard, our analysis resembles ψ-analysis, in which helix-stabilizing metal ion-binding sites are introduced into proteins (35), thereby allowing the overall stability of the protein to be

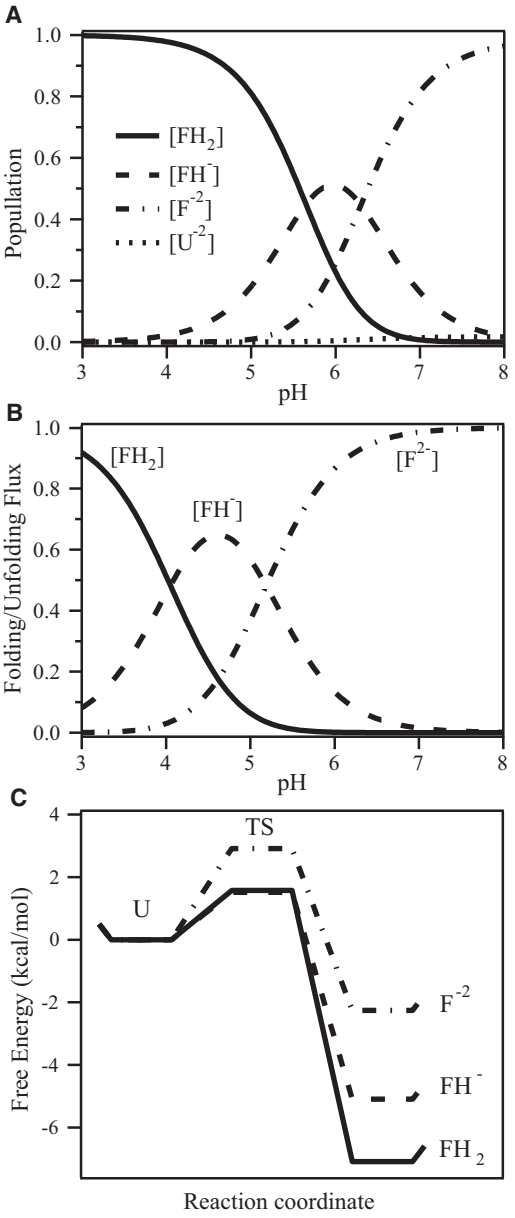

FIGURE 4 (*A*) Plots of calculated populations (mole fraction) of the folded states (FH_2, FH^-, and F^{-2}) versus pH in the absence of denaturant. The unfolded states (*dotted line*) have negligible population under these conditions. Populations were calculated from the kinetic parameters in Table 1. (*B*) Flux of molecules through the three parallel channels in the six-state scheme (Fig. 1 *D*), defined as the product of folded population in each charge state and the corresponding unfolding rate constant, normalized with respect to the total flux. (*C*) Schematic free-energy profiles for the conformational transitions of the three charge states of GCN4-D. A preexponential factor $A = 1 \times 10^6\ \mathrm{s}^{-1}$ was used for calculating the free energy of the folding transitions state, $\Delta G^{\ddagger}_f = -RT\cdot\ln(k_f/A)$.

continuously varied by varying the concentration of the metal ion. The major difference between the two approaches is that tertiary interactions rather than secondary structure is probed in this work. Nevertheless, we find similar phenomena; by raising or lowering the stability of a specific region of the protein, it becomes possible to reshape the transition state ensemble for folding.

The observed inverse correlation between $\alpha^{\ddagger}$ and unfolding free energy (Table 1) suggests that structure formation in the transition state compensates for the decrease in stability due to the loss of favorable hydrogen bonding and/or electrostatic interactions involving Asp^{18}. Taking the results of the Φ-value and $\alpha^{\ddagger}$ analysis together, we conclude that during folding of the fully protonated coiled-coil (FH_2), the specific interactions between the Asp^{18} and $Asp^{18\prime}$ side chains are formed only after crossing the rate-limiting barrier. This conclusion is consistent with the mutational analysis by Knappenberger et al. (36). On the other hand, our observation of a Φ-value of 0.5 when comparing the doubly-charged to the singly-charged species indicates that the transition state encountered during folding of the F^{-2} species experiences charge repulsion that raises the free energy not only for the F^{-2} state, but also for the folding barrier, implying that the Asp^{18} side chains on each half of the linked dimer are partially interacting in the transition-state ensemble. This suggests a scenario in which a partially structured transition-state ensemble favors highly efficient folding (at rates of at least 60,000 s^{-1}) of the fully and singly-protonated species, most likely by a zipper mechanism starting from the cross-linked C-terminus. In the case of the fully deprotonated species, charge repulsion interferes with this zipper mechanism, resulting in a much slower rate of folding (5500 s^{-1}). To be productive, the transition-state ensemble must then become more product-like by acquiring additional stabilizing interactions before it can traverse the rate-limiting barrier. Evidence for such Hammond behavior (64,65) has also been observed in designed coiled-coils with Glu residues at more solvent-exposed e- and g-positions of the coiled-coil (66). Alternatively, the transition-state ensemble of F^{-2} might also consist of a heterogeneous population of fully structured and completely unfolded states.

A plot of the predicted equilibrium populations for each of the six states versus pH in the absence of denaturant (Fig. 4 *A*) shows that the neutral folded form, FH_2, is dominant at acidic pH (<4) while the fully deprotonated species (F^{-2}) is the predominant state at basic pH (>7). All three charge states contribute to the folded population at intermediate pH values. The fact that the population of unfolded molecules is negligible for all charge states, together with the observation that the CD signal at 222 nm varies little with pH (Fig. 2), indicates that folded coiled-coil structure of GCN4-D is largely unperturbed even in the presence of one or two buried charges at position 18. This is consistent with previous findings that ionizable side chains are tolerated with minimal conformational changes at many interior sites of stable globular proteins (6), and only rarely lead to local unfolding (67,68). The protonation state of Asp^{18} determines the flux through alternative parallel folding pathways. Fig. 4 *B* shows the contribution of each charge state to folding/unfolding flux as defined by the normalized product of the equilibrium population of each state in the folded state and the rate constants for unfolding of each charged state (as expected for a reversible system at equilibrium, identical results were obtained when we calculated the flux in the folding direction). It can be seen that the F^{-2} state contributes disproportionately to the kinetics (relative to its equilibrium population in the folded ensemble), because its rate of unfolding is significantly faster than that of the other states.

Our findings indicate that hydrogen-bonded interactions of a solvent-shielded polar residue are important not only for the stability and specificity of the GCN4 coiled-coil structure, but can also modulate the rate of folding by shaping an intrinsically heterogeneous transition-state ensemble. In addition, this study illustrates the use of protein engineering and quantitative kinetic analysis in unraveling microscopic features of complex protein folding mechanisms.

SUPPORTING MATERIAL

Three figures and additional information on modeling of equilbrium and kinetic data are available at http://www.biophysj.org/biophysj/supplemental/S0006-3495(10)00933-1.

The work was supported by grants from the National Institutes of Health (No. GM056250 to H.R. and No. GM54616 to W.F.D.), a grant from the National Cancer Institute (No. CA06927), and an Appropriation by the Commonwealth of Pennsylvania to the Fox Chase Cancer Center.

REFERENCES

1. Tanford, C. 1980. The Hydrophobic Effect. John Wiley & Sons, New York.
2. Makhatadze, G. I., and P. L. Privalov. 1995. Energetics of protein structure. *Adv. Protein Chem.* 47:307–425.
3. Dill, K. A. 1990. Dominant forces in protein folding. *Biochemistry.* 29:7133–7155.
4. Tanford, C. 1970. Protein denaturation. C. Theoretical models for the mechanism of denaturation. *Adv. Protein Chem.* 24:1–95.
5. Yang, A. S., M. R. Gunner, …, B. Honig. 1993. On the calculation of pK_as in proteins. *Proteins.* 15:252–265.
6. Isom, D. G., B. R. Cannon, …, B. García-Moreno. 2008. High tolerance for ionizable residues in the hydrophobic interior of proteins. *Proc. Natl. Acad. Sci. USA.* 105:17784–17788.
7. Doyle, D. A., J. Morais Cabral, …, R. MacKinnon. 1998. The structure of the potassium channel: molecular basis of K^+ conduction and selectivity. *Science.* 280:69–77.
8. Yoshikawa, S., K. Shinzawa-Itoh, …, T. Tsukihara. 1998. Redox-coupled crystal structural changes in bovine heart cytochrome *c* oxidase. *Science.* 280:1723–1729.

9. Fersht, A. R. 1999. Structure and Mechanism in Protein Science: A Guide to Enzyme Catalysis and Protein Folding. W.H. Freeman, Cambridge, UK.
10. Luecke, H., and J. K. Lanyi. 2003. Structural clues to the mechanism of ion pumping in bacteriorhodopsin. *Adv. Protein Chem.* 63:111–130.
11. Baker, E. N., and R. E. Hubbard. 1984. Hydrogen bonding in globular proteins. *Prog. Biophys. Mol. Biol.* 44:97–179.
12. Scholtz, J. M., H. Qian, …, R. L. Baldwin. 1993. The energetics of ion-pair and hydrogen-bonding interactions in a helical peptide. *Biochemistry.* 32:9668–9676.
13. Kortemme, T., A. V. Morozov, and D. Baker. 2003. An orientation-dependent hydrogen bonding potential improves prediction of specificity and structure for proteins and protein-protein complexes. *J. Mol. Biol.* 326:1239–1259.
14. Grigoryan, G., and W. F. Degrado. 2008. Modest membrane hydrogen bonds deliver rich results. *Nat. Chem. Biol.* 4:393–394.
15. Harbury, P. B., T. Zhang, …, T. Alber. 1993. A switch between two-, three,- and four-stranded coiled coils in GCN4 leucine zipper mutants. *Science.* 262:1401–1407.
16. Gonzalez, Jr., L., D. N. Woolfson, and T. Alber. 1996. Buried polar residues and structural specificity in the GCN4 leucine zipper. *Nat. Struct. Biol.* 3:1011–1018.
17. Akey, D. L., V. N. Malashkevich, and P. S. Kim. 2001. Buried polar residues in coiled-coil interfaces. *Biochemistry.* 40:6352–6360.
18. Marqusee, S., and R. T. Sauer. 1994. Contributions of a hydrogen bond/salt bridge network to the stability of secondary and tertiary structure in λ-repressor. *Protein Sci.* 3:2217–2225.
19. James, M. N., and A. R. Sielecki. 1986. Molecular structure of an aspartic proteinase zymogen, porcine pepsinogen, at 1.8 Å resolution. *Nature.* 319:33–38.
20. Fitzgerald, P. M., and J. P. Springer. 1991. Structure and function of retroviral proteases. *Annu. Rev. Biophys. Biophys. Chem.* 20:299–320.
21. Shoichet, B. K., W. A. Baase, …, B. W. Matthews. 1995. A relationship between protein stability and protein function. *Proc. Natl. Acad. Sci. USA.* 92:452–456.
22. Shi, Z., B. A. Krantz, …, T. R. Sosnick. 2002. Contribution of hydrogen bonding to protein stability estimated from isotope effects. *Biochemistry.* 41:2120–2129.
23. Phelan, P., A. A. Gorfe, …, H. R. Bosshard. 2002. Salt bridges destabilize a leucine zipper designed for maximized ion pairing between helices. *Biochemistry.* 41:2998–3008.
24. Whitten, S. T., B. E. García-Moreno, and V. J. Hilser. 2008. Ligand effects on the protein ensemble: unifying the descriptions of ligand binding, local conformational fluctuations, and protein stability. *Methods Cell Biol.* 84:871–891.
25. Pace, C. N., G. R. Grimsley, and J. M. Scholtz. 2009. Protein ionizable groups: pK values and their contribution to protein stability and solubility. *J. Biol. Chem.* 284:13285–13289.
26. Marti, D. N., and H. R. Bosshard. 2004. Inverse electrostatic effect: electrostatic repulsion in the unfolded state stabilizes a leucine zipper. *Biochemistry.* 43:12436–12447.
27. Matousek, W. M., B. Ciani, …, A. T. Alexandrescu. 2007. Electrostatic contributions to the stability of the GCN4 leucine zipper structure. *J. Mol. Biol.* 374:206–219.
28. Marti, D. N., and H. R. Bosshard. 2003. Electrostatic interactions in leucine zippers: thermodynamic analysis of the contributions of Glu and His residues and the effect of mutating salt bridges. *J. Mol. Biol.* 330:621–637.
29. Yadav, M. K., L. J. Leman, …, M. R. Ghadiri. 2006. Coiled coils at the edge of configurational heterogeneity. Structural analyses of parallel and antiparallel homotetrameric coiled coils reveal configurational sensitivity to a single solvent-exposed amino acid substitution. *Biochemistry.* 45:4463–4473.
30. Deng, Y., Q. Zheng, …, M. Lu. 2007. Self-assembly of coiled-coil tetramers in the 1.40 Å structure of a leucine-zipper mutant. *Protein Sci.* 16:323–328.
31. Zitzewitz, J. A., O. Bilsel, …, C. R. Matthews. 1995. Probing the folding mechanism of a leucine zipper peptide by stopped-flow circular dichroism spectroscopy. *Biochemistry.* 34:12812–12819.
32. Sosnick, T. R., S. Jackson, …, W. F. DeGrado. 1996. The role of helix formation in the folding of a fully α-helical coiled coil. *Proteins.* 24:427–432.
33. Zitzewitz, J. A., B. Ibarra-Molero, …, C. R. Matthews. 2000. Preformed secondary structure drives the association reaction of GCN4-p1, a model coiled-coil system. *J. Mol. Biol.* 296:1105–1116.
34. Ibarra-Molero, B., G. I. Makhatadze, and C. R. Matthews. 2001. Mapping the energy surface for the folding reaction of the coiled-coil peptide GCN4-p1. *Biochemistry.* 40:719–731.
35. Krantz, B. A., and T. R. Sosnick. 2001. Engineered metal binding sites map the heterogeneous folding landscape of a coiled coil. *Nat. Struct. Biol.* 8:1042–1047.
36. Knappenberger, J. A., J. E. Smith, …, C. R. Matthews. 2002. A buried polar residue in the hydrophobic interface of the coiled-coil peptide, GCN4-p1, plays a thermodynamic, not a kinetic role in folding. *J. Mol. Biol.* 321:1–6.
37. Ibarra-Molero, B., J. A. Zitzewitz, and C. R. Matthews. 2004. Salt-bridges can stabilize but do not accelerate the folding of the homodimeric coiled-coil peptide GCN4-p1. *J. Mol. Biol.* 336:989–996.
38. Lee, D. L., S. Ivaninskii, …, R. S. Hodges. 2003. Unique stabilizing interactions identified in the two-stranded α-helical coiled-coil: crystal structure of a cortexillin I/GCN4 hybrid coiled-coil peptide. *Protein Sci.* 12:1395–1405.
39. Schneider, J. P., J. D. Lear, and W. F. DeGrado. 1997. A designed buried salt bridge in a heterodimeric coiled coil. *J. Am. Chem. Soc.* 119:5742–5743.
40. Fersht, A. R., A. Matouschek, and L. Serrano. 1992. The folding of an enzyme. I. Theory of protein engineering analysis of stability and pathway of protein folding. *J. Mol. Biol.* 224:771–782.
41. Moran, L. B., J. P. Schneider, …, T. R. Sosnick. 1999. Transition state heterogeneity in GCN4 coiled coil folding studied by using multisite mutations and crosslinking. *Proc. Natl. Acad. Sci. USA.* 96:10699–10704.
42. Roder, H., and W. Colón. 1997. Kinetic role of early intermediates in protein folding. *Curr. Opin. Struct. Biol.* 7:15–28.
43. Oas, T. G., L. P. McIntosh, …, P. S. Kim. 1990. Secondary structure of a leucine zipper determined by nuclear magnetic resonance spectroscopy. *Biochemistry.* 29:2891–2894.
44. Straussman, R., A. Ben-Ya'acov, …, S. Ravid. 2007. Kinking the coiled coil—negatively charged residues at the coiled-coil interface. *J. Mol. Biol.* 366:1232–1242.
45. Testa, O. D., E. Moutevelis, and D. N. Woolfson. 2009. CC+: a relational database of coiled-coil structures. *Nucleic Acids Res.* 37 (Database issue):D315–D322.
46. Lee, H. H., N. Elia, …, J. H. Hurley. 2008. Midbody targeting of the ESCRT machinery by a noncanonical coiled coil in CEP55. *Science.* 322:576–580.
47. Wagschal, K., B. Tripet, …, R. S. Hodges. 1999. The role of position a in determining the stability and oligomerization state of α-helical coiled coils: 20 amino acid stability coefficients in the hydrophobic core of proteins. *Protein Sci.* 8:2312–2329.
48. O'Shea, E. K., K. J. Lumb, and P. S. Kim. 1993. Peptide 'Velcro': design of a heterodimeric coiled coil. *Curr. Biol.* 3:658–667.
49. Krylov, D., I. Mikhailenko, and C. Vinson. 1994. A thermodynamic scale for leucine zipper stability and dimerization specificity: E and G interhelical interactions. *EMBO J.* 13:2849–2861.
50. Lumb, K. J., and P. S. Kim. 1995. Measurement of interhelical electrostatic interactions in the GCN4 leucine zipper. *Science.* 268:436–439.
51. Yu, Y., O. D. Monera, …, P. L. Privalov. 1996. Ion pairs significantly stabilize coiled-coils in the absence of electrolyte. *J. Mol. Biol.* 255:367–372.

52. Wendt, H., L. Leder, …, H. R. Bosshard. 1997. Very rapid, ionic strength-dependent association and folding of a heterodimeric leucine zipper. *Biochemistry.* 36:204–213.

53. Dutta, K., A. Alexandrov, …, S. M. Pascal. 2001. pH-induced folding of an apoptotic coiled coil. *Protein Sci.* 10:2531–2540.

54. Acharya, A., S. B. Ruvinov, …, C. Vinson. 2002. A heterodimerizing leucine zipper coiled coil system for examining the specificity of a position interactions: amino acids I, V, L, N, A, and K. *Biochemistry.* 41:14122–14131.

55. Dutta, K., F. A. Engler, …, S. M. Pascal. 2003. Stabilization of a pH-sensitive apoptosis-linked coiled coil through single point mutations. *Protein Sci.* 12:257–265.

56. Bosshard, H. R., D. N. Marti, and I. Jelesarov. 2004. Protein stabilization by salt bridges: concepts, experimental approaches and clarification of some misunderstandings. *J. Mol. Recognit.* 17:1–16.

57. Meisner, W. K., and T. R. Sosnick. 2004. Barrier-limited, microsecond folding of a stable protein measured with hydrogen exchange: implications for downhill folding. *Proc. Natl. Acad. Sci. USA.* 101:15639–15644.

58. Meisner, W. K., and T. R. Sosnick. 2004. Fast folding of a helical protein initiated by the collision of unstructured chains. *Proc. Natl. Acad. Sci. USA.* 101:13478–13482.

59. Bosshard, H. R., E. Dürr, …, I. Jelesarov. 2001. Energetics of coiled coil folding: the nature of the transition states. *Biochemistry.* 40:3544–3552.

60. Matouschek, A., J. T. Kellis, Jr., …, A. R. Fersht. 1989. Mapping the transition state and pathway of protein folding by protein engineering. *Nature.* 340:122–126.

61. de los Rios, M. A., B. K. Muralidhara, …, I. Ruczinski. 2006. On the precision of experimentally determined protein folding rates and ϕ-values. *Protein Sci.* 15:553–563.

62. Bunagan, M. R., L. Cristian, …, F. Gai. 2006. Truncation of a cross-linked GCN4-p1 coiled coil leads to ultrafast folding. *Biochemistry.* 45:10981–10986.

63. Wang, T., W. L. Lau, …, F. Gai. 2005. T-jump infrared study of the folding mechanism of coiled-coil GCN4-p1. *Biophys. J.* 89:4180–4187.

64. Matouschek, A., D. E. Otzen, …, A. R. Fersht. 1995. Movement of the position of the transition state in protein folding. *Biochemistry.* 34:13656–13662.

65. Sánchez, I. E., and T. Kiefhaber. 2003. Non-linear rate-equilibrium free energy relationships and Hammond behavior in protein folding. *Biophys. Chem.* 100:397–407.

66. Dürr, E., I. Jelesarov, and H. R. Bosshard. 1999. Extremely fast folding of a very stable leucine zipper with a strengthened hydrophobic core and lacking electrostatic interactions between helices. *Biochemistry.* 38:870–880.

67. Karp, D. A., A. G. Gittis, …, B. García-Moreno E. 2007. High apparent dielectric constant inside a protein reflects structural reorganization coupled to the ionization of an internal Asp. *Biophys. J.* 92:2041–2053.

68. Zheng, Z., and T. R. Sosnick. 2010. Protein vivisection reveals elusive intermediates in folding. *J. Mol. Biol.* 397:777–788.